The NMR Structure of the *Staphylococcus aureus* Response Regulator VraR DNA Binding Domain Reveals a Dynamic Relationship between It and Its Associated Receiver Domain[†]

Logan W. Donaldson*

Department of Biology, York University, 4700 Keele Street, Toronto, Ontario M3J 1P3, Canada

Received September 10, 2007; Revised Manuscript Received January 8, 2008

ABSTRACT: In *Staphylococcus aureus*, a two-component signaling system consisting of the histidine kinase VraS and the response regulator VraR stimulates gene expression in response to antibiotics that inhibit cell wall formation. With respect to understanding the mechanism of the VraSR response and precise interaction of VraR at promoter sites, the structure of the VraR DNA binding domain (DBD) was determined using NMR methods. The DBD demonstrates a four-helix configuration that is shared with the NarL/FixJ family of response regulators and is monomeric in solution. Unobservable amide resonances in VraR NMR spectra coincided with a set of DNA backbone contact sites predicted from a model of a VraR−DNA complex. This observation suggests that a degree of conformational sampling is required to achieve a high-affinity interaction with DNA. On the basis of chemical shift differences and line broadening, an amino-terminal 3_{10} helix and a portion of helix H4 identify a continuous surface that may link the DBD to the receiver domain. The full-length VraR protein thermally denatured with a single transition, suggesting that the receiver domain and DBD were integrated and not simply tethered. Of note, the DBD alone denatured at a temperature that was 21 °C higher than that of the full-length protein. Thus, the DBD appears to be thermodynamically and structurally sensitive to state of the receiver domain.

A cell-wall-stress stimulon of more than 100 genes is activated in methicillin resistant *Staphylococcus aureus* (MRSA) and vancomycin resistant *S. aureus* (VRSA) upon exposure to antibiotics (*1*–*6*). In addition to enzymes involved in cell wall biosynthesis such as FmtA, MurZ, and Pbp2, the cell-wall-stress stimulon is represented by proteins with diverse roles in amino acid transport, carbohydrate transport, DNA repair, lipid metabolism, and post-translation modification (*4*). Understanding how these proteins function together represents a critical step toward creating therapeutic approaches to combating *S. aureus* infections, particularly in clinical settings.

One of the key sentinels (*7*) that monitors cell wall changes in MRSA and VRSA is a classic, two-component signaling system (*8*–*10*) composed of the histidine kinase VraS and its response regulator VraR. Approximately one-third of the cell-wall-stress stimulon is regulated by VraSR, including *vraSR* itself (*3*). VraR is transcribed as part of a 2.7 kb message containing *vraS*, the gene encoding its sensor kinase partner and two open reading frames of unknown function, *yvqF* and *orf1* (*45*). In *Bacillus subtilis*, an operon with a similar although not identical composition has been observed (*11*), suggesting that in many species of bacteria, VraSR-like operons can be configured to suit a range of signaling events. Indeed, a BLAST search identifies more than 100 homologous bacterial proteins with sequences at least 40% identical to that of VraR.

This report begins by presenting the structure of the VraR C-terminal DNA binding domain (DBD)[1] that was determined by nuclear magnetic resonance (NMR) methods. Chemical shift differences between the DBD alone and in its native context within full-length VraR identified the dimerization helix as the bridge between the DBD and the N-terminal receiver (or phosphoacceptor) domain. Many unobservable resonances were noted in NMR spectra of the full-length protein, suggesting that the inactive and active states of VraR are in a dynamic equilibrium at a micro- to millisecond time scale. A complementary circular dichroism (CD) study was performed with solutions of the DBD, full-length VraR, and VraR treated with beryllofluoride (BeF_3^-) to mimic the active, phosphorylated state. From this study, the DBD was observed to be more thermostable alone than when it was integrated with the receiver domain. Using a molecular model of a dimeric VraR DBD−DNA complex as a starting point, the possible DNA binding properties of VraR are presented.

EXPERIMENTAL PROCEDURES

Cloning and Expression. In the Mu50 strain of *S. aureus*, VraR is designated as open reading frame SAV1884. Gene fragments encoding full-length VraR (1–209), the receiver domain (1–133), and the DNA binding domain (138–209)

[†] This work was supported by the Natural Sciences and Engineering Research Council of Canada (Discovery Grant 238934-6) with salary support by the Canadian Institutes of Health Research.

* E-mail: logand@yorku.ca. Phone: (416) 736-2100, ext. 22823. Fax: (416) 736-5698.

[1] Abbreviations: DBD, DNA binding domain; FL, full-length; NMR, nuclear magnetic resonance; rmsd, root-mean-square deviation.

10.1021/bi701844q CCC: $40.75
Published on Web 02/23/2008

were PCR-amplified Mu50 genomic DNA obtained from ATCC (Rockville, MD) and inserted into the *Nde*I and *Bam*HI sites of pET15b (Novagen). All expressed proteins had a 19-residue His_6 affinity tag and thrombin protease cleavage site appended to the amino terminus. Milligram quantities of isotopically labeled VraR proteins were produced from a 1 L fermentation of *Escherichia coli* BL21:DE3 at 37 °C in M9 minimal medium supplemented with 1 g/L [^{15}N]ammonium chloride and 4 g/L [^{13}C]glucose as the sole nitrogen and carbon sources, respectively. The VraR DBD was expressed as a soluble fusion protein. Cell lysates dissolved in T500 buffer [10 mM Tris-HCl (pH 8.0), 500 mM NaCl, and 0.05% NaN_3] were clarified by centrifugation at 30000*g* for 15 min with the soluble extract proceeding directly to the chromatographic purification stage. In contrast, the full-length VraR fusion protein was expressed in inclusion bodies and required a brief refolding procedure, as follows. The harvested bacterial pellet was resuspended in 15 mL of 8 M guanidinium hydrochloride and incubated at room temperature for 30 min. Following centrifugation at 30000*g* for 15 min to remove insoluble debris, the supernatant containing the denatured protein was rapidly diluted into 600 mL of cold T500 buffer. Prior to chromatography, the renatured protein solution was clarified by centrifugation at 30000*g* for 10 min. To purify the His_6-tagged, full-length VraR and VraR DBD, protein solutions were applied to ~10 mL of Ni-NTA resin (Qiagen). Following a wash with 10 mM imidazole in T500 buffer, the VraR protein was eluted with 20 mM EDTA in T500 buffer. The purified protein solution was concentrated to 4 mL and subjected to gel filtration chromatography using a Sephacryl S100 16/60 column (GE Biosciences) to achieve further purification and exchange the protein into a NMR compatible buffer.

Chemical Modifications. To mimic the phosphorylated state, solutions of full-length VraR protein were treated with a 5-fold molar excess of $BeCl_2$ (Sigma-Aldrich) and a 50-fold molar excess of NaF. Protein cross-linking was performed by incubating 20 μM protein solutions with 0.08% glutaraldehyde. Reactions were halted by adding a solution consisting of 250 mM Tris-HCl (pH 8.0) and sodium dodecyl sulfate/glycerol/dithiothreitol gel loading buffer. Cross-linked proteins were resolved by electrophoresis under denaturing conditions and stained with Coomassie Blue.

NMR Spectroscopy and Structure Determination. Both full-length VraR and the VraR DBD proteins were stable in a NMR buffer composed of 10 mM sodium phosphate (pH 7.8), 750 mM NaCl, 10 mM $MgCl_2$, 0.05% NaN_3, and 10% D_2O. Even at high salt concentrations, both preparations of VraR demonstrated concentration- and temperature-dependent aggregation. The full-length VraR was stable at a concentration of 0.3 mM for only days at 35 °C. The VraR DBD at a concentration of 0.6 mM was stable for weeks at 35 °C. All NMR experiments were performed on a 600 MHz Varian NMR instrument equipped with a single-axis, pulsed field gradient, cryogenically cooled Gen3 salt tolerant probe. Samples were ~300 μL in volume and enclosed in susceptibility-matched 3 mm × 6 mm S-tubes (Shigemi). Standard Varian BioPack pulse sequences were employed. The majority of backbone assignments were obtained by using the PINE server at NMRFAM/University of Wisconsin (http://miranda.nmrfam.wisc.edu/PINE) with peak tables from two-dimensional (2D) ^{15}N HSQC, three-dimensional (3D) HNCACB, 3D CBCA(CO)NH, and 3D HNCO spectra as input. Side chain assignments were obtained from a combined analysis of 2D ^{13}C HSQC, 3D H(CCO)NH, 3D C(CO)NH, and 3D HCCH-TOCSY spectra. Aromatic ring assignments were obtained from a combined analysis of 2D (HB)CB(CGCD)HD, 2D (HB)CB(CGCDCE)HE, and 3D aromatic HCCH-TOCSY spectra. NOE distance restraints were obtained from 3D ^{15}N HSQC-NOESY (100 ms mixing time), 3D ^{13}C HSQC-NOESY (100 ms), and 3D aromatic ^{13}C HSQC-NOESY (100 ms) spectra. Data were processed and interpreted using nmrPipe (*12*) and NMRView (*13*). No stereospecific assignments were made. All geminal protons were made ambiguous prior to structure calculations. NOE distance restraints were calibrated from 2.4 to 5.0 Å using CYANA 2.1 (*14*). Hydrogen bond restraints (O–HN, 1.8–2.1 Å; O–N, 2.7–3.0 Å) were determined by assessing the initial ensemble for backbone O–HN distances of <2.4 Å and bond angles of <25°. Backbone dihedral angles (ψ and φ) were predicted from chemical shift information using the PREDITOR method (*15*). An initial ensemble of 250 structures was calculated with CYANA 2.1. The top 25 lowest-energy structures were refined in explicit solvent (*16*) with XPLOR-NIH 2.18.0 (*17*) to produce a final ensemble of 10 lowest-energy structures.

Structural Analysis and Bioinformatics. Ramachandran analysis of an ensemble of 10 lowest-energy structures was performed using PROCHECK-NMR (*18*). Ensemble rmsds were calculated with MOLMOL (*19*). The EBI SSM server (*20*) was used to identify structurally similar proteins in the Protein Data Bank and to perform 3D pairwise comparisons. Secondary structure predictions were performed using the PROF method (http://www.predictprotein.org). Amide chemical shift perturbations were calculated using a weighted method that accounts for the ~10-fold difference between ^{1}H and ^{15}N gyromagnetic ratios $\{\Delta\delta = [(\Delta\delta_H)^2 + 0.01(\Delta\delta_N)^2]^{0.5}\}$.

Data Deposition. Coordinates and restraint lists were deposited in the Protein Data Bank as entry 2RNJ. Chemical shift assignments were deposited in the BioMagResBank as entry 11024.

NMR Dynamics. Amide ^{15}N T_1 relaxation spectra were acquired with delays of 10, 30, 50, 110, 210, 310, and 510 ms. Amide ^{15}N T_2 relaxation spectra were acquired with delays of 10, 30, 50, 70, 90, and 110 ms. Resonances were integrated and normalized with the nLinLS module of the NMRDraw software suite. Amide ^{15}N T_1 and T_2 relaxation times were calculated from least-squares fitting to a monoexponential function. A molecular rotational correlation time was calculated using a Mathematica notebook written by P. Mercier (Chenomx, Edmonton, AB) employing a subset of the relaxation data whose T_1/T_2 ratios were all within one standard deviation.

Circular Dichroism Spectroscopy. Far-UV spectra of VraR proteins at a concentration of 20 μM in the NMR buffer were acquired with a Jasco J-810 instrument. A rectangular cell with a path length of 0.1 cm was used for all measurements. Spectra were recorded from 250 to 200 nm with a scan rate of 50 nm/min and a 1.0 nm bandwidth and subtracted from a solvent blank. Protein concentrations were calculated from an absorbance at 280 nm and an extinction coefficient predicted by the ProtParam server at http://www.expasy.org. A midpoint denaturation temperature (T_m) was determined

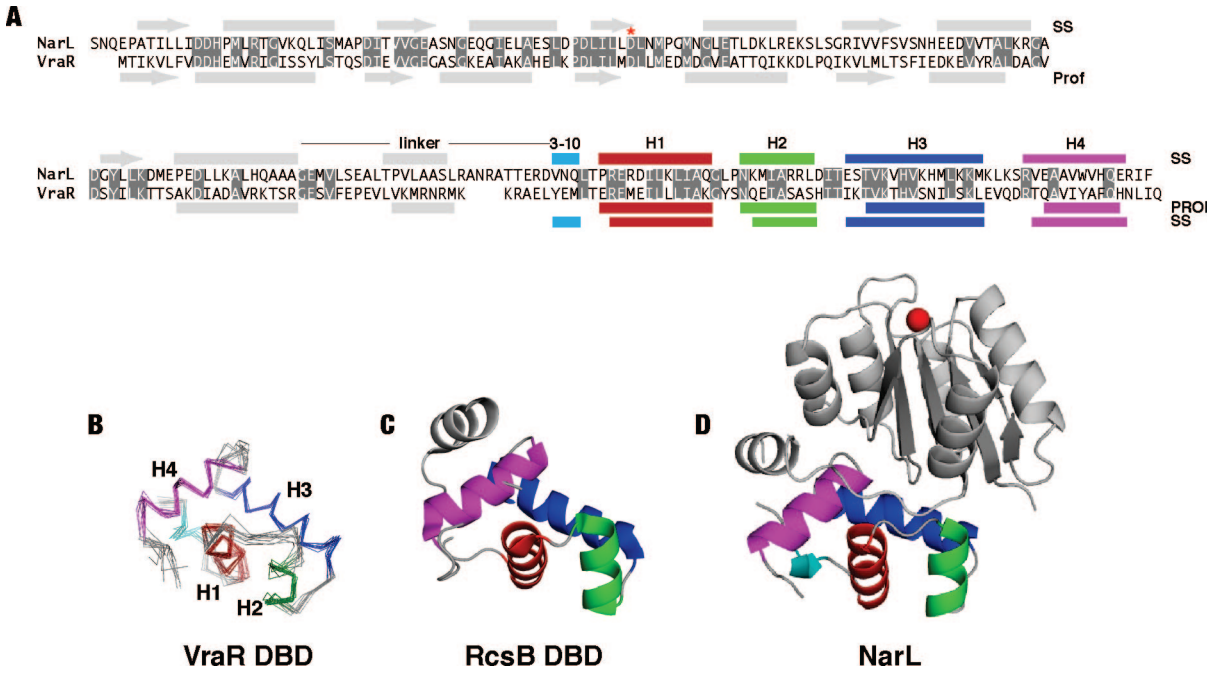

FIGURE 1: Structural and sequence similarity of VraR with related bacterial response regulators. (A) Sequence alignment of VraR with the transcription factor NarL. Sequence identity between the two proteins is indicated. Secondary structure (SS) elements above the NarL sequence are derived from the crystal structure. Secondary structure elements depicted below the VraR sequence are derived from either a secondary structure prediction (PROF, from the server at www.predictprotein.org) or the NMR structure of the DNA binding domain. (B) A Cα trace of the 10 lowest-energy structures of the VraR DBD. (C) A structurally similar four-helix DBD from the *Erwinia amylovora* transcriptional regulator RcsB. This DBD is characterized by an additional C-terminal helix that is colored gray. (D) In contrast to RcsB, an additional helix in NarL is situated N-terminally with respect to the DNA binding domain but occurs in an analogous position.

by heating samples from 20 to 90 at a rate of 1 °C/min and monitoring ellipticity at 222 nm, a wavelength that is diagnostic for α-helical content.

Analytical Gel Filtration. A 20 μM solution of the full-length VraR or VraR DBD was applied to a Superdex-75 10/30 HR gel filtration column (GE Biosciences) equilibrated in NMR buffer and pumped at 0.5 mL/min. Eluted proteins were detected by the absorbance at 280 nm. Chromatograms of molecular weight standards (GE Biosciences) were acquired during the same session.

Molecular Modeling. The crystal structure of the dimeric DosR DBD−DNA complex (PDB entry 1ZLK) served as a template for the initial stage of model building. Each DosR monomer was replaced with the VraR NMR structure by least-squares coordinate superposition using ProFit (A. Martin, SciTech Software). Since the VraR-specific DNA binding site is unknown, the DosR DNA duplex sequence (5′-TTTGGGGACTAAAGTCCCTAAC-3′/5′-GTTAGGGACTTTAGTCCCCAAA-3′) was retained for the modeling. Steric clashes and deviations from ideal geometry were minimized using an adapted water refinement protocol (*16*) for XPLOR-NIH. During the refinement, the VraR protein component was restrained by the same NOE, dihedral angle, and hydrogen bond restraints that were used to determine the NMR structure. The DNA duplex was refined with 108 Watson–Crick hydrogen bond distance restraints, 480 dihedral angle restraints, 22 base planarity restraints, and a potential derived from a multidimensional nucleic acid conformational database (*21*). Intermolecular protein–protein and protein−DNA contacts were defined by 41 ambiguous restraints with a maximum distance of 2.5 Å and no lower boundary. These intermolecular restraints were analogous to the AIRs used by the HADDOCK approach (*22*). Molecular graphics were produced with PyMOL (http://pymol.sourceforge.net).

RESULTS

Protein Expression. VraR is very similar in sequence to *E. coli* NarL (*23, 24*), a transcription factor that is phosphorylated by the sensor histidine kinases NarX and NarQ in response to varying concentrations of nitrate and nitrite. As a result, VraR is predicted to retain a similar architecture consisting of an N-terminal phosphoacceptor (or receiver) domain and a C-terminal DNA binding domain (DBD) separated by an ∼20-residue linker region (Figure 1a). Although expressed full-length His_6-tagged VraR was found in the insoluble fraction of *E. coli* lysates, it could be readily and quantitatively refolded from denaturant. Excellent chemical shift dispersion in amide $^1H-^{15}N$ HSQC spectra of full-length VraR suggested that the refolding procedure produced native protein.

Using sequence similarity as a guide, the amino-terminal receiver domain was expressed as a His_6-tagged fusion protein. This protein fragment was expressed in the insoluble fraction of *E. coli* and could not be refolded from denaturant. In contrast, a longer His_6-tagged protein fragment containing the receiver domain and the linker region (amino acids 1–133) could be refolded from denaturant as determined from qualitative inspection of amide HSQC spectra (data not presented). This deletion suggests that the linker region supplies critical hydrophobic contacts and possibly additional structural elements to the receiver domain.

Like that of the receiver domain, NMR spectroscopy of full-length VraR could be performed on samples only at low

Table 1: Statistics for the Ensemble of Structures of the *S. aureus* VraR DNA Binding Domain[a]

no. of unique distance restraints	
intraresidue	319
sequential ($i - j = 1$)	112
medium-range ($2 \leq i - j \leq 4$)	51
long-range ($i - j \geq 4$)	100
hydrogen bond pairs (HN−O, N−O)	17
NOE violations	
>0.3 Å	5.8 ± 1.8
>0.1 Å	37.0 ± 3.7
dihedral angle restraints[b]	
φ and ψ angles for each amino acid	50
deviations from standard geometry (XPLOR-NIH)	
bonds	0.0105 ± 0.0005
angles	1.3753 ± 0.0383
impropers	1.6617 ± 0.1618
dihedral angles	0.2970 ± 0.1308
pairwise rmsd	
secondary structures[c]	
backbone	0.73 ± 0.13 Å
all heavy atoms	1.53 ± 0.15 Å
all atoms[d]	
backbone	0.87 ± 0.14 Å
all heavy atoms	1.78 ± 0.17 Å
Ramachandran statistics[e]	
most favored regions	89.8%
additional allowed regions	8.8%
generously allowed regions	0.5%
disallowed regions	0.9%

[a] Ensemble of the top 10 structures with the lowest overall energy and no NOE violations of >0.5 Å. [b] Predicted from chemical shifts using the PREDITOR web server. [c] The rmsd values for residues 145–147, 151–160, 166–172, 176–190, and 196–205. [d] The rmsd values for residues 145–205. [e] Determined with PROCHECK-NMR for the ensemble, not including dihedral angles of residues 150, 151, 165, 166, 173, and 175, for which no amide assignments were available.

concentrations in the presence of at least 0.5 M NaCl. These conditions precluded a full NMR structural investigation but did allow some higher-sensitivity experiments such as 3D HNCA to be performed.

In stark contrast, a fragment of VraR encompassing a portion of the linker region and the DBD (amino acids 138–209) was expressed well in the soluble fraction of *E. coli* and was stable for weeks at 35 °C when the protein concentration did not exceed 0.6 mM and the NaCl concentration was at least 0.5 M. Under these conditions, a suite of standard triple-resonance experiments were performed that were sufficient to determine the structure of the VraR DBD.

Structural Attributes of the DNA Binding Domain. The NMR structure of the VraR DBD was calculated from a set of 582 unique NOE distance restraints and 50 dihedral angle restraints predicted from chemical shifts (Table 1). Over the ensemble of the 10 lowest-energy structures, the backbone atom rmsd for the secondary structural elements was 0.73 Å (Figure 1B). The VraR DBD demonstrates a typical four-helix fold that is shared by the bacterial transcription factors NarL (*25*), FixJ (*26*), RcsB (*27*), DosR (*28*), GerE (*29*), and TraR (*30–32*). Cα atom rmsds between VraR and these structures range from 1.11 to 2.33 Å (Table 2). Each of the four helices (H1–H4) in the DBD can be ascribed a general role in activation (H1), scaffolding (H2), DNA recognition (H3), or dimerization (H4).

The N-terminal His_6 affinity tag and linker residues M138−L144 were deemed to be disordered since no resonances could be assigned. Immediately after this region, the first contributions to the hydrophobic core are made by Y145–L148. These residues situated at the end of the linker form a short 3_{10} helix. In the FixJ DBD, the 3_{10} helix is replaced by a 10-residue α helix at the same position (*26*). The remaining hydrophobic contacts in the structure are derived from the four helices of the VraR DBD (Y145, L148, I155, L156, I159, Y163, I168, V179, V183, V186, L187, L190, A198, A202, and L207). Supporting their role in the hydrophobic core, the residues are identified by an above average number of NOEs. Figure S1 of the Supporting Information provides a per-residue distribution of the NOEs used in the structure calculation. The scaffolding (H2) and recognition (H3) helices form a typical helix−turn−helix motif that is fused via hydrophobic interactions between I168 and V179. The short side chain of A169 identifies the point at which helix H2 and helix H3 cross each other. As amide resonances of H173 and I176 in the "turn" of the VraR HTH motif were not observed, a degree of conformational sampling may be required for VraR to bind its promoter site.

The DBD of RcsB hosts an additional, flanking helix located at its C-terminus (Figure 1C). In NarL, this flanking helix is preserved in an analogous position but is instead found N-terminal to the DBD (Figure 1D). By its degree of sequence similarity to NarL, a flanking helix in VraR is predicted to occur N-terminal to the DBD from V133 to K139. As the VraR protein fragment used in the structural study did not include these residues, it was not possible to determine if V133−K139 support a flanking helix. However, since the hydrophobic core of the DBD appears to be complete, it suggests that the presence of a flanking helix in the linker region may have another function unrelated to DNA binding in full-length VraR.

Activated State of VraR. The full-length NarL response regulator has been determined in two crystal forms (*23, 24*). In each case, the receiver domain and DBD were observed as one structural unit as opposed to two tethered, independent domains. From the perspective of the DBD, the interface between the two domains envelops a portion of helix H3 and helix H4. Thus, in its inactive, unphosphorylated state, the NarL−DNA interaction is weakened. It is not known precisely how phosphorylation of D59 in NarL (and D55 by homology, in VraR) propagates a signal across the receiver domain to release the DBD. However, prior NMR investigations have demonstrated that phosphorylation can modulate the relative populations of the inactive and active forms of NarL (*33*).

While response regulators are widely known to accept phosphate from phosphoramidate (*33*) and other low-molecular weight donors such as acetyl phosphate (*34*) and carbamyl phosphate (*35*), the susceptibility of the phosphorylated aspartic acid to hydrolysis complicates biophysical studies. In lieu, VraR solutions were treated with a beryllofluoride (BeF_3^-), a compound that binds tightly to the receiver domain and mimics the phosphorylated state (*36–42*).

Oligomeric State of VraR. Although early crystallographic studies supported dimerization of NarL (*23*), the archetype of the family to which VraR belongs, later NMR studies demonstrated that the isolated NarL receiver domain and DBD were monomeric in solution (*33*). As a first step toward determining the oligomeric state of VraR and the DBD, analytical gel filtration was performed (Figure 2). According to the standard curve that was employed, the observed retention times of His_6-tagged VraR, His_6-tagged VraR

Table 2: Structural Similarity[a] between the *S. aureus* VraR DBD and Other Bacterial Four-Helix DBDs

source	PDB	method	no. of amino acids aligned	% similarity	Cα rmsd	ref
Mycobacterium tuberculosis DosR	1ZLJ:B	X-ray	60	37	1.11	*28*
M. tuberculosis DosR and DNA	1ZLK:B	X-ray	61	36	1.33	*28*
E. coli NarL	1ZG1:E	X-ray	64	25	1.58	*25*
Sinorhizobium meliloti FixJ	1X3U:A	NMR	65	23	1.81	*26*
E. amylovora RcsB	1P4W:A	NMR	65	26	1.93	*27*
Agrobacterium tumefaciens TraR	1H0M:A	X-ray	59	20	2.33	*30*
B. subtilis GerE	1FSE:C	X-ray	53	38	2.33	*29*

[a] Performed with the EBI SSM server (http://www.ebi.ac.uk/msd-srv/ssm).

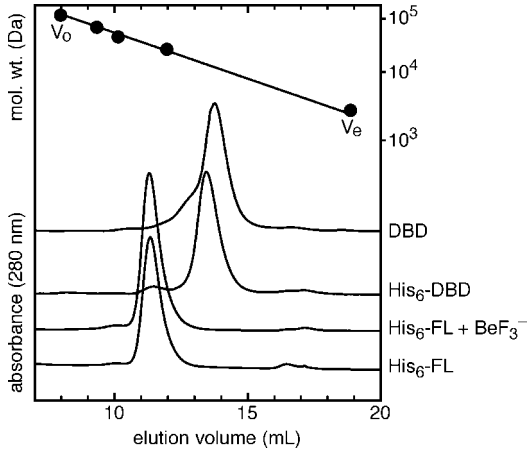

FIGURE 2: Gel filtration chromatograms of full-length VraR, BeF_3^--treated VraR, and the VraR DNA binding domain (DBD). Each protein sample was at a concentration of 10 μM in 250 μL. A plot of molecular weight vs elution volume is shown above the chromatograms. The void volume (V_o, 120 kDa) and maximum elution volumes (V_e, 3 kDa) were determined with solutions of blue dextran and salt. Additional calibrations were made with albumin (67 kDa), ovalbumin (43 kDa), and chymotrypsin (25 kDa).

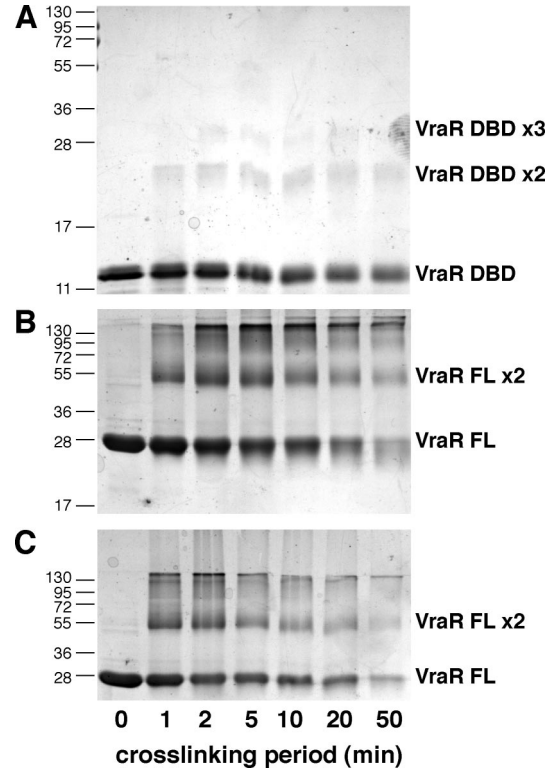

FIGURE 3: Chemical cross-linking. Each 20 μM sample of (A) the VraR DBD, (B) full-length VraR, and (C) BeF_3^--treated VraR was treated with 0.08% glutaraldehyde for the periods shown. Cross-linked products were resolved by denaturing gel electrophoresis.

treated with beryllofluoride, and the His_6-tagged DBD all overestimated the expected molecular weight by 30–50%. When the 19-residue affinity tag was removed from the DBD with thrombin, only a minor change in the retention time was observed. This result suggests that the affinity tag does not perturb the hydrodynamics of the DBD, even when it contributes more than 20% of the total mass.

From amide ^{15}N T_1 and T_2 relaxation rate analyses performed at 25 °C, the calculated correlation times of the affinity-tagged and untagged VraR DBD were 8.5 and 8.4 ns, respectively. Corroborating the gel filtration study, these correlation times were more consistent with a 10 kDa monomer than a 20 kDa dimer.

Chemical cross-linking was performed to identify the oligomeric state of full-length VraR and the DBD in dilute solutions. After incubation for 50 min with glutaraldehyde, the DBD remained essentially monomeric when resolved on a denaturing polyacrylamide gel (Figure 3). A similar treatment applied to VraR and beryllofluoride-treated VraR produced bands corresponding to dimers and possibly tetramers within 1 min of exposure to glutaraldehyde. The proportion of oligomeric VraR did not increase with longer cross-linking periods. Rather, an increase in a very high molecular weight species that could not enter the gel was observed, suggesting that the cross-linking reagent was exacerbating the tendency of VraR to aggregate over time. No precipitate was observed during the cross-linking period. Considered together, the gel filtration and chemical cross-linking studies suggest that VraR is predominantly monomeric in its inactive and activated states.

Intra- and Interdomain Dynamics. Amide $^1H-^{15}N$ HSQC spectra of the VraR DBD demonstrated line widths that were characteristic of a 10 kDa protein fragment. When the HSQC spectra of the DBD and full-length VraR were overlaid, many similar resonances were observed, suggesting that the structure of the DBD in the full-length protein was retained.

As the period between two alternating conformational states becomes comparable to the chemical shift differences (in hertz) of the resonances occupying each state, line broadening will increase to a point were the resonances become unobservable. Fluctuations on the order of micro- to milliseconds are sufficient to produce extreme line broadening. Approximately 160 of 205 possible amide resonances were observed in the HSQC spectrum of full-length VraR, suggesting that micro- to millisecond dynamics were occurring at one or more sites.

Amide resonance assignments of the DBD in full-length VraR were made using a combination of 3D HNCA and 3D ^{15}N-edited NOESY spectra. A ^2H-, ^{13}C-, and ^{15}N-labeled

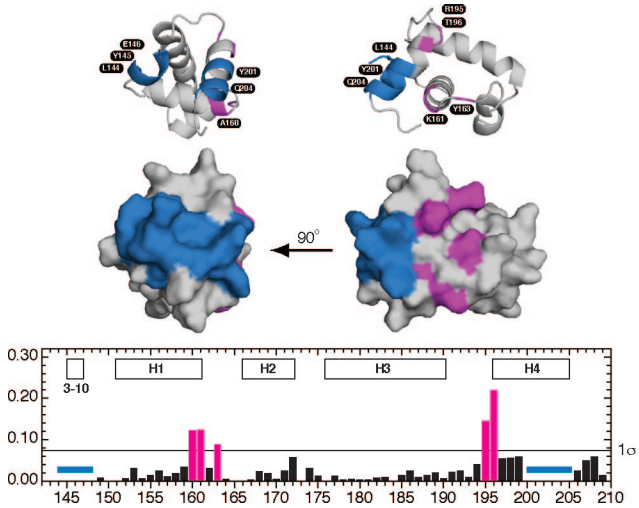

FIGURE 4: Chemical shift mapping the interaction surface between the DBD and receiver domain. Amide chemical shift differences greater than one standard deviation (1σ) from the mean difference are colored magenta. Unobservable amide resonances from the amino terminal 3_{10} helix and helix H4 are colored blue and indicated by horizontal bars in the chart.

sample of full-length VraR was also prepared to facilitate a complete backbone assignment. However, the sensitivity gains obtained by perdeuteration were not sufficient to overcome the experimental limitations imposed by poor sample solubility.

Each pair of ^{1}H and ^{15}N chemical shifts contributing to a given amide resonance represents a sensitive probe of the local chemical and magnetic environment. In Figure 4, weighted $^{1}H-^{15}N$ chemical shift differences measured from HSQC spectra of the DBD alone and full-length VraR were charted and mapped onto the DBD structure. The largest chemical shift changes localized to portions of helix H1 and the H3−H4 loop. Despite an exhaustive search of the full-length VraR HNCA and ^{15}N NOESY data sets, no amide resonances were observed for the region encompassing the 3_{10} helix (L144−L148) and a large portion of helix H4 (I200−H205). Combined, the unobservable resonances and the chemical shift changes form a contiguous surface. If this surface is presumed to be the binding site for the receiver domain, the exposed hydrophobic side chains of Y145, V199, I200, and Y201 may facilitate the association.

Upon addition of BeF_3^-, the amide HSQC spectrum of VraR demonstrated even fewer resonances. By visual inspection, the majority of the remaining resonances were attributed to the DBD. HSQC spectra of the VraR DBD, full-length VraR, and beryllofluoride-treated VraR are presented together as Figure S2 of the Supporting Information.

Thermal Stability of VraR. Solutions of the DBD and full-length VraR in its inactive and activated states were investigated using circular dichroism (CD) spectroscopy. From the far-UV spectra shown in Figure 5, both the DBD and the full-length protein demonstrate a trough at 222 nm that is characteristic of a protein with high helical content (52% for the His_6-tagged DBD, 53% for the His_6-tagged full-length VraR). Qualitatively, the relative differences in the CD spectra of VraR and beryllofluoride-treated VraR suggest that phosphorylation promotes a conformation change that may involve release of the DBD from the receiver domain.

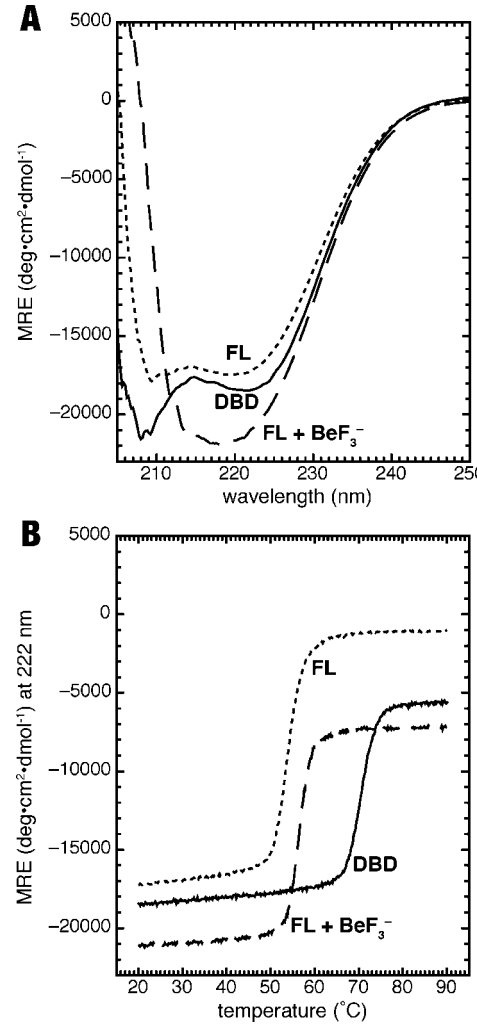

FIGURE 5: Circular dichroism (CD) spectroscopy. (A) Far-UV CD spectra of full-length (FL) VraR, beryllofluoride-treated VraR (FL + BeF_3^-), and the VraR DBD. (B) Thermal denaturation profiles of VraR solutions monitored at 222 nm.

A thermal denaturation midpoint (T_m) was determined for each VraR solution. As expected for a single domain, the DBD demonstrated a denaturation profile with a single transition at 73 °C. In contrast, full-length VraR and beryllofluoride-treated VraR also denatured with a single transition, but at much lower temperatures of 52 and 54 °C, respectively.

Molecular Modeling of the VraR−DNA Complex. The consensus NarL binding site is an inverted heptameric repeat of TAC(C/T)(C/T)(C/A)T that is separated by 2 bp (*43*). This configuration presents the major groove binding sites of each heptamer on the same face of DNA. In the open, DNA-bound conformation of NarL, bases in the major groove are contacted by the helix−turn−helix motifs (helix H2 and helix H3) of the two DBDs and a tight dimer is formed (*25, 44*). While NarL would have served as a suitable starting point for molecular modeling of VraR, the crystal structure of the *M. tuberculosis* DosR−DNA complex (*28*) was chosen instead because of its higher degree of sequence similarity, particularly throughout the recognition helix. The VraR DBD sequence was threaded into the DosR crystal structure with no gaps and refined to produce the model shown in Figure 6. As the DNA binding site of VraR is unknown, the DosR-specific DNA sequence was not altered.

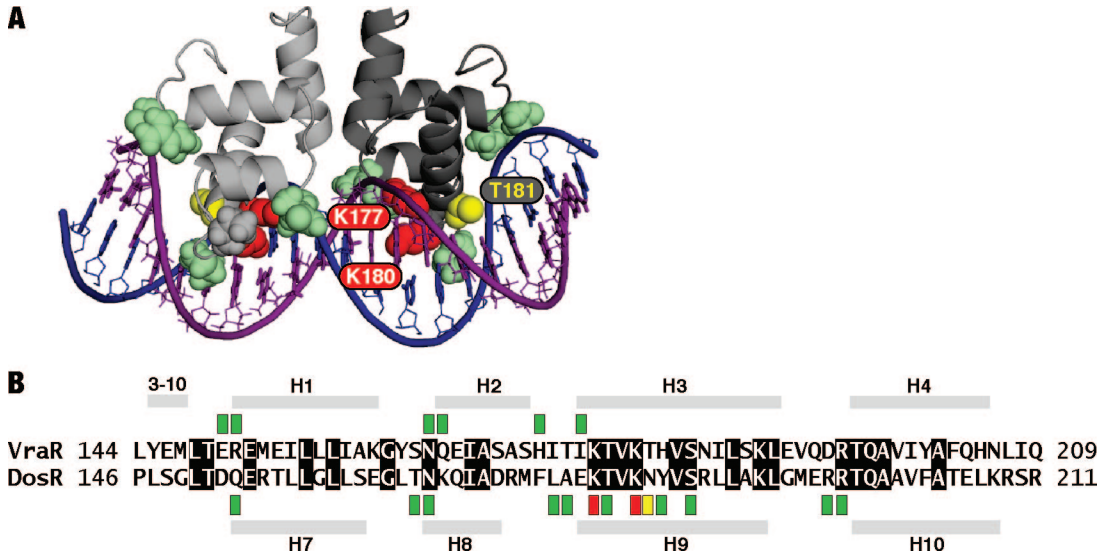

FIGURE 6: Molecular modeling of the VraR DBD−DNA interaction. (A) Two VraR DNA binding domains were docked and refined with a 20 bp imperfect, inverted repeat dsDNA sequence derived from the crystal structure of the DosR−DNA complex (PDB entry 1ZLK). Three residues of the recognition helix (K177, K180, and T181, in space-filling representation) are predicted to make base-specific interactions. Many of the unobservable amide resonances in HSQC spectra of the VraR DBD correspond with DNA backbone contact sites (green, in space-filling representation). (B) Sequence alignment of the VraR and DosR DBDs. Green squares above the VraR denote missing resonances. Green squares below the DosR sequence denote observed sugar–phosphate contacts in the crystal structure.

One DosR monomer contacts the DNA half-site with the sequence $G_1G_2G_3A_4C_5T_6$. Base-specific DNA binding by the recognition helix of DosR is achieved with three residues (K179, K182, and N183). In VraR, the first two residues are preserved (K177 and K180) with T181 substituting for N183 in DosR. In a survey of the model, the first lysine (K177) makes base discriminatory contacts with G_3 and flanking contacts with G_2 and A_4. The second lysine (K182) interacts with the C_5 and T_6 base pairs. The amino group of either cytosine in the G_1 or G_2 base pair is positioned to make a hydrogen bond with N183 of DosR. As observed in the model of the VraR DBD−DNA complex, a substitution of G_1 and G_2 with A_1 and A_2, respectively, would position thymine methyl groups for complementary van der Waals contacts with the T181 side chain. With these substitutions in mind, a possible palindromic consensus sequence for VraR becomes AAGACTNNAGTCTT. From reporter gene studies, VraR promotes transcription of its own operon from a sequence bounded by base pairs −262 to +150 relative to the major transcription start point (*45*). A survey of this region identifies a partial palindrome at position −71 with the sequence AAGACTaaAGTaTg. Further studies are required to determine if this sequence can support transcription by VraR.

Six residues located throughout the VraR DBD could not be assigned because of unobservable amide resonances. Although these residues appear to be unremarkable in their position throughout the VraR sequence, a pattern emerges when they are considered in a structural context. As shown in Figure 6, these residues correspond to predicted DNA backbone contact sites in the model of the VraR DBD−DNA complex. In dynamic terms, local motions on the intermediate time scale may help the DBD fine-tune its interaction with DNA or help scan tracts of DNA for an optimal binding site.

DISCUSSION

Because of its involvement in the expression of more than one-third of the genes involved in the primary response to cell wall damage, VraR presents a useful starting point for understanding the systems biology of antibiotic response in *S. aureus*. Emphasizing its central role in antibiotic resistance, constitutive VraR expression in MRSA strain N315 (*2*) was sufficient to increase the minimal inhibitory concentration of vancomycin from 0.5 to 2 μg/mL (*1*). Recently, a 4-fold increase in vancomycin resistance in a *S. aureus* isolate from a patient undergoing antibiotic therapy was correlated with a mutation in *yvqF*, a putative transporter gene located in the *vraSR* operon (*6*).

Residing on a mobile chromosomal cassette, the *mecA* gene encodes PBP2a, a penicillin binding protein conferring resistance to the β-lactam antibiotics methicillin and oxacillin, among others (*46*). While VraSR does not appear to affect *mecA* expression directly, *vraSR* transcription levels are correlated with the production of PBP2, one of four endogenous penicillin binding proteins whose activity is known to complement PBP2a (*7*). Even if *pbp2* expression is decoupled from VraSR, VraSR is still required (*45, 47*). Taken together with the observation that sensitivity to methicillin can be restored in clinically relevant strains bearing a knockout in *Vras*, the VraRS operon is clearly an essential conduit for the expression of genes involved in antibiotic resistance (*45*).

This paper presents the first biochemical investigation of VraR and the first structural investigation of its DNA binding domain (DBD). The VraR DBD demonstrates a four-helix topology that is typical of the NarL/FixJ structural class. Previous X-ray and NMR studies of NarL identified the recognition helix of the DBD as the primary contact site to the receiver domain. In contrast, chemical shift differences between the VraR DBD and receiver domain identify a surface that draws contributions from a short 3_{10} helix and helix H4.

The crystal structure of NarL suggested a "telephone receiver" model of activation in which the DNA binding domain is released from the receiver domain upon phosphorylation of a specific aspartic acid (*24*). As shown in Figure 1, the recognition helix (H3) is bound to the receiver domain in a manner that would prevent DNA binding. In contrast, chemical shift changes presented in this report identify the dimerization helix (H4) and a structured portion of the linker as the interface to the VraR receiver domain. The potential difference in the juxtaposition of the two domains does not imply that a telephone receiver model of activation is invalid for VraR. The same conformational changes occurring in the receiver domain that promote an open, DNA-accessible state may simply be directed toward a different surface of the DBD.

From a combination of analytical gel filtration, chemical cross-linking, and NMR relaxation approaches, full-length VraR, beryllofluoride-activated VraR, and the DBD alone were determined to be predominantly monomeric in solution. Like NarL, the VraR response regulator is predicted to dimerize only when it binds an inverted repeat DNA sequence. Other response regulators from the OmpR/PhoB and DctD/NtrC families dimerize upon phosphorylation in the absence of DNA.

Base-specific contacts between NarL and DNA are made by the amino acid triad Ser/Lys/Val of the recognition helix (*44*). The sole lysine at the second position is predicted to be versatile with respect to the number and kind of bases that it can read out. At the third position in the NarL, a relatively bulky valine side chain creates a signature base pair distortion in its vicinity (*25*). As VraR presents a threonine at the third position of the triad, the geometry of the DNA may be more canonical as observed in the DosR−DNA complex with a Lys/Lys/Asn triad. Although no experimental evidence is currently available, the VraR DBD may recognize other types of heptameric binding sites. NarL, for example, interacts with single heptamers and tandem repeats with different functional outcomes (*25*). As a detailed survey of VraR promoter regions has not been performed, it remains unknown if VraR can modulate transcription from single heptameric sequences.

In the model of the VraR−DNA complex, local and global conformational changes in the DNA arising from specific base contacts are supported by numerous nonspecific contacts with the sugar–phosphate backbone. Residues situated throughout the VraR DBD that were predicted to make these nonspecific contacts were distinguished by unobservable amide resonances. Two of the unobservable amide resonances in VraR (N165 and R195) were also unobservable at similar positions in the NarL DBD (N173 and R203), suggesting micro- to millisecond fluctuations in DNA-interacting regions may be a general hallmark of the four-helix family of bacterial DNA binding domains.

NMR studies of Spo0F and NtrC response regulators identify intermediate time scale dynamics as an important functional attribute. In Spo0F, amides exhibiting chemical exchange rates of $>20\ s^{-1}$ coincide with the phosphoacceptor site and the docking surface for its effector kinases. Thus, conformational sampling in Spo0F ensures that protein binding is coupled with efficient phospho transfer (*48*). In NtrC, chemical exchange occurs at sites that experience the most conformational changes upon phosphorylation (*49*). Rather than considering NtrC in terms of discrete inactive and active states, an allosteric model describing NtrC as a population of conformations in equilibrium was determined to be more appropriate (*50, 51*).

NMR studies of NarL have shown that the receiver domain and DBD can associate in *trans*, albeit with a low dissociation constant (K_d) of ~100 μM (*33*). Because they are tethered by a short linker in native NarL, the effective concentration of the receiver domain and DBD is greatly increased. This has the effect of shifting the equilibrium in NarL toward the inactive conformation. In agreement with a model that predicts a weakened interdomain interaction upon phosphorylation, the K_d of receiver domain−DBD interaction was observed to decrease 100-fold upon addition of phosphoramidate (*33*). Like those of NarL, the two domains of VraR are intimately associated as full-length VraR thermally denatures with a single transition. Strikingly, the DBD alone denatured at a temperature that was 21 °C higher than that of the full-length protein. Rather than the DBD stabilizing the receiver domain, the receiver domain appeared to destabilize the DBD. Functionally, this outcome may be desirable since conformational and thermodynamic changes occurring in the receiver domain will then have consequences for both domains. It is currently not known if a longer linker is sufficient to destabilize the VraR DNA binding domain.

A relatively large set of missing amide resonances in the HSQC spectra of full-length VraR indicates that micro- to millisecond dynamics contribute to the equilibrium between the inactive and active states. Further work is being performed to identify mutants that affect this equilibrium and improve the solution characteristics of full-length VraR for additional NMR and crystallographic studies.

ACKNOWLEDGMENT

Dr. Dasantila Golemi-Kotra and Antoaneta Belcheva are acknowledged for sharing their unpublished data. I am particularly grateful to Dr. Imogen Coe and Dr. Arthur Hilliker for their encouragement while I completed this project on my sabbatical leave.

SUPPORTING INFORMATION AVAILABLE

Chart of the NOEs used for the VraR DBD structure calculation on a per-residue basis (Figure S1) and HSQC spectra of the VraR DBD, full-length VraR, and beryllofluoride-activated VraR (Figure S2). This material is available free of charge via the Internet at http://pubs.acs.org.

REFERENCES

1. Kuroda, H., Kuwahara-Arai, K., and Hiramatsu, K. (2000) Identification of the up- and down-regulated genes in vancomycin-resistant *Staphylococcus aureus* strains Mu3 and Mu50 by cDNA differential hybridization method. *Biochem. Biophys. Res. Commun. 269*, 485–490.
2. Kuroda, H., Ohta, T., Uchiyama, I., Baba, T., Yuzawa, H., and Kobayashi, I. (2001) Whole genome sequencing of methicillin-resistant *Staphylococcus aureus*. *Lancet 357*, 1225–1240.
3. Kuroda, M., Kuroda, H., Oshima, F., Takeuchi, F., Mori, H., and Hiramatsu, K. (2003) Two-component system VraSR positively modulates the regulation of cell-wall biosynthesis pathway in *Staphylococcus aureus*. *Mol. Microbiol. 49*, 807–821.
4. Utaida, S., Dunman, P. M., Macapagal, D., Murphy, E., Projan, S. J., Singh, R. K., Jayaswal, R. K., and Wilkinson, B. J. (2003) Genome-wide transcriptional profiling of the response of *Staphy-*

lococcus aureus to cell-wall-active antibiotics reveals a cell-wall-stress stimulon. *Microbiology 149*, 2719–2732.
5. McAleese, F., Wu, S. W., Sieradzki, K., Dunman, P. M., Murphy, E., Projan, S. J., and Tomasz, A. (2006) Overexpression of genes of the cell wall stimulon in clinical isolates of *Staphylococcus aureus* exhibiting vancomycin-intermediate *S. aureus*-type resistance to vancomycin. *J. Bacteriol. 188*, 1120–1133.
6. Mwangi, M. M., Wu, S.-W., Zhou, Y., Sieradzki, K., de Lencastre, H., Richardson, P., Bruce, D., Rubin, E., Myers, E., Siggia, E. D., and Tomasz, A. (2007) Tracking the in vivo evolution of multidrug resistance in *Stapylococcus aureus* by whole-genome sequencing. *Proc. Natl. Acad. Sci. U.S.A. 104*, 9451–9456.
7. Gardete, S., Wu, S. W., Gill, S., and Tomasz, A. (2006) Role of VraSR in antibiotic resistance and antibiotic-induced stress response in *Staphylococcus aureus*. *Antimicrob. Agents Chemother. 50*, 3424–3434.
8. West, A. H., and Stock, A. M. (2001) Histidine kinases and response regulator proteins in two-component signaling systems. *Trends Biochem. Sci. 26*, 369–376.
9. Fabret, C., Feher, V. A., and Hoch, J. A. (1999) Two-component signal transduction in *Bacillus subtilis*: How one organism sees the world. *J. Bacteriol. 181*, 1975–1983.
10. Stock, A. M., Robinson, V. L., and Goudreau, P. N. (2000) Two-component signal transduction. *Annu. Rev. Biochem. 69*, 183–215.
11. Wipat, A., Brignell, S. C., Guy, B. J., Rose, M., Emmerson, P. T., and Harwood, C. R. (1998) The yvsA-yvqA (293°−289°) region of the *Bacillis subtilis* chromosome containing genes involved in metal ion uptake and a putative sigma factor. *Microbiology 144*, 1593–1600.
12. Delaglio, F., Grzesiek, S., Vuister, G. W., Zhu, G., Pfeifer, J., and Bax, A. (1995) NMRPipe: A multidimensional spectral processing system based on UNIX pipes. *J. Biomol. NMR 6*, 277–293.
13. Johnson, B. A., and Blevins, R. A. (1994) NMRVIEW: A computer program for the visualization and analysis of NMR data. *J. Biomol. NMR 4*, 603–614.
14. Guntert, P. (2004) Automated NMR structure calculation with CYANA. *Methods Mol. Biol. 278*, 353–378.
15. Berjanskii, M. V., Neal, S., and Wishart, D. S. (2006) PREDITOR: A web server for predicting protein torsion angle restraints. *Nucleic Acids Res. 34*, W63–W69.
16. Linge, J. P., Williams, R. M., Spronk, C. A., Bonvin, A. M., and Nilges, M. (2003) Refinment of protein structures in explicit solvent. *Proteins 50*, 496–506.
17. Schweiters, C. D., Kuzewski, J. J., Tjandra, N., and Clore, G. M. (2003) The XPLOR-NIH molecular structure determination package. *J. Magn. Reson. 160*, 66–74.
18. Laskowski, R., Rullman, J., MacArthur, M., Kaptein, R., and Thornton, J. (1996) AQUA and PROCHECK-NMR: Programs for checking the quality of protein structures solved by NMR. *J. Biomol. NMR 8*, 477–486.
19. Koradi, R., Billeter, M., and Wuthrich, K. (1996) MOLMOL: A program for display and analysis of macromolecular structures. *J. Mol. Graphics 14*, 51–55.
20. Krissinel, E., and Henrick, K. (2004) Secondary-structure matching (SSM), a new tool for fast protein structure alignment in three dimensions. *Acta Crystallogr. D60*, 2256–2268.
21. Kuszewski, J., and Clore, G. M. (2000) Sources of and solutions to problems in the refinement of protein NMR structures against torsion angle potentials of mean force. *J. Magn. Reson. 146*, 249–254.
22. Dominguez, C., Boelens, R., and Bonvin, A. M. (2003) HADDOCK: A protein-protein docking approach based on biochemical or biophysical information. *J. Am. Chem. Soc. 125*, 1731–1737.
23. Baikalov, I., Schroder, I., Kaczor-Grzeskowiak, M., Cascio, D., Gunsalus, R. P., and Dickerson, R. E. (1998) NarL dimerization? Suggestive evidence from a new crystal form. *Biochemistry 37*, 3665–3676.
24. Baikalov, I., Schroder, I., Kaczor-Grzeskowiak, M., Grzeskowiak, K., Gunsalus, R. P., and Dickerson, R. E. (1996) Structure of the *Escherichia coli* response regulator NarL. *Biochemistry 35*, 11053–11061.
25. Maris, A. E., Kaczor-Grzeskowiak, M., Ma, Z., Kopka, M. L., Gunsalus, R. P., and Dickerson, R. E. (2005) Primary and secondary modes of DNA recognition by the NarL two-component response regulator. *Biochemistry 44*, 14538–14552.
26. Kurashima-Ito, K., Kasai, Y., Hosono, K., Tamura, K., Oue, S., Isogai, M., Ito, Y., Nakamura, H., and Shiro, Y. (2005) Solution structure of the C-terminal transcriptional activator domain of FixJ from *Sinorhizobium meliloti* and its recognition of the fixK promoter. *Biochemistry 44*, 14835–14844.
27. Pristovsek, P., Sengupta, K., Lohr, F., Schafer, B., von Trebra, M. W., Ruterjans, H., and Bernhard, F. (2003) Structural analysis of the DNA-binding domain fo the *Erwinia amylovora* RcsB protein and its interaction with the RcsAB box. *J. Biol. Chem. 278*, 17752–17759.
28. Wisedchaisri, G., Wu, M., Rice, A. E., Roberts, D. M., Sherman, D. R., and Hol, W. G. J. (2005) Structures of *Mycobacterium tuberculosis* DosR and DosR-DNA complx involved in gene activation during adapation to hypoxic latency. *J. Mol. Biol. 354*, 630–641.
29. Ducros, V. M., Lewis, R. J., Verma, C. S., Dodson, E. J., Leonard, G., Turkenberg, J. P., Murshudov, G. N., Wilkinson, B. J., and Brannigan, J. A. (2001) Crystal structure of GerE, the ultimate transcriptional regulator of spore formation in *Bacillus subtilis*. *J. Mol. Biol. 306*, 759–771.
30. Vannini, A., Volpari, C., and Di Marco, S. (2004) Crystal structure of the quorum-sensing protein TraM and its interaction with the transcriptional regulator TraR. *J. Biol. Chem. 279*, 24291–24296.
31. Zhang, R. G., Pappas, T., Brace, J. L., Miller, P. C., Oulmassov, T., Molyneaux, J. M., Anderson, J. C., Bashkin, J. K., Winans, S. C., and Joachimiak, A. (2002) Structure of a bacterial quorum-sensing transcription factor complexed with pheromone and DNA. *Nature 417*, 971–974.
32. White, C. E., and Winans, S. C. (2007) The quorum-sensing transcription factor TraR decodes its DNA binding site by direct contacts with DNA bases and by detection of DNA flexibility. *Mol. Microbiol.,* 245–256.
33. Eldridge, A. M., Kang, H. S., Johnson, E., Gunsalus, R., and Dahlquist, F. W. (2002) Effect of phosphorylation on the interdomain interaction of the response regulator, NarL. *Biochemistry 41*, 15173–15180.
34. Lukat, G. S., McCleary, W. R., Stock, A. M., and Stock, J. B. (1992) Phosphorylation of bacterial response regulator proteins by low molecular weight phospho-donors. *Proc. Natl. Acad. Sci. U.S.A. 89*, 718–722.
35. Lowry, D. F., Roth, A. F., Rupert, P. B., Dahlquist, F. W., Moy, F. J., Domaille, P. J., and Matsumura, P. (1994) Signal transduction in chemotaxis. A propagating conformation change upon phosphorylation of CheY. *J. Biol. Chem. 269*, 26358–26362.
36. Wemmer, D. E., and Kern, D. (2005) Beryllofluoride binding mimics phosphorylation of aspartate in response regulators. *J. Bacteriol. 187*, 8229–8230.
37. Yan, D., Cho, H. S., Hastings, C. A., Igo, M. M., Lee, S. Y., Pelton, J. G., Stewart, V., Wemmer, D. E., and Kustu, S. (1999) Beryllofluoride mimics phosphorylation of NtrC and other bacterial response regulators. *Proc. Natl. Acad. Sci. U.S.A. 96*, 14789–14794.
38. Cho, H., Wang, W., Kim, R., Yokota, H., Damo, S., Kim, S.-H., Wemmer, D., Kustu, S., and Yan, D. (2001) BeF_3^- acts as a phosphate analog in proteins phosphorylated on aspartate: Structure of a BeF_3^- complex with phosphoserine phosphatase. *Proc. Natl. Acad. Sci. U.S.A. 98*, 8525–8530.
39. Riepl, H., Scharf, B., Schmitt, R., Kalbitzer, H. R., and Maurer, T. (2004) Solution structures of the inactive and BeF_3^- activated response regulator CheY2. *J. Mol. Biol. 338*, 287–297.
40. Nixon, B. T., Yannawar, H. P., Doucleff, M., Pelton, J. G., Wemmer, D., Krueger, S., and Kondrashkina, E. (2005) SAS solutions structures of the Apo and Mg^{2+}/BeF_3^- bound receiver domain of DctD from *Sinorhizobium meliloti*. *Biochemistry 44*, 13962–13969.
41. Toro-Roman, A., Mack, T. R., and Stock, A. M. (2005) Structural analysis and solution studies of the activated regulatory domain of the response regulator ArcA: A symmetric dimer mediated by the α4-β5-α5 face. *J. Mol. Biol. 349*, 11–26.
42. Bachhawat, P., and Stock, A. M. (2007) Crystal structures of the receiver domain of response regulator PhoP from *Escherichia coli* in the absence and presence of the phosphoryl analog beryllofluoride. *J. Bacteriol. 189*, 5987–5995.
43. Li, J., Kustu, S., and Stewart, V. (1994) In vitro interaction of nitrate-responsive regulatory protein NarL with DNA target sequences in the fdnG, narG, narK and frdA operon control regions of *Escherichia coli* K-12. *J. Mol. Biol. 241*, 150–165.
44. Maris, A. E., Sawaya, M. R., Kaczor-Grzeskowiak, M., Jarvis, M. R., Bearson, S. M., Kopka, M. L., Schroder, I., Gunsalus, R. P., and Dickerson, R. E. (2002) Dimerization allows DNA target site recognition by the NarL response regulator. *Nat. Struct. Biol. 9*, 771–778.
45. Yin, S., Daum, R. S., and Boyle-Vavra, S. (2006) VraSR two-component regulatory system and its role in induction of *pbp2* and

vraSR expression by cell wall antimicrobials in *Staphylococcus aureus*. *Antimicrob. Agents Chemother. 50*, 336–343.
46. Deresinki, S. (2005) Methicillin-resistant *Staphylococcus aureus*: An evolutionary, epidemiologic and therapeutic odyssey. *Clin. Infect. Dis. 40*, 562–573.
47. Boyle-Vavra, S., Yin, S., and Daum, R. S. (2006) The VraS/VraR two-component regulatory system required for oxacillin resistance in community-acquired methicillin-resistant *Staphylococcus aureus*. *FEMS Microbiol. Lett. 262*, 163–171.
48. Feher, V. A., and Cavanagh, J. (1999) Millisecond-timescale motions contribute to the function of the bacterial response regulator protein SpoOF. *Nature 400*, 289–293.
49. Volkman, B. F., Lipson, D., Wemmer, D. E., and Kern, D. (2001) Two-state allosteric behavior in a single-domain signaling protein. *Science 291*, 2429–2433.
50. Hu, X., and Wang, Y. (2006) Molecular dynamic simulations of the N-terminal receiver domain of NtrC reveal intrinsic conformational flexibility in the inactive state. *J. Biomol. Struct. Dyn. 23*, 509–518.
51. Gardino, A. K., and Kern, D. (2007) Functional dynamics of response regulators using NMR relaxation techniques. *Methods Enzymol. 423*, 149–165.

BI701844Q